We are IntechOpen, the world's leading publisher of Open Access books Built by scientists, for scientists

4,800
Open access books available

122,000
International authors and editors

135M
Downloads

Our authors are among the

154
Countries delivered to

TOP 1%
most cited scientists

12.2%
Contributors from top 500 universities

CLARIVATE ANALYTICS BOOK CITATION INDEX INDEXED

WEB OF SCIENCE™

Selection of our books indexed in the Book Citation Index in Web of Science™ Core Collection (BKCI)

Interested in publishing with us?
Contact book.department@intechopen.com

Numbers displayed above are based on latest data collected.
For more information visit www.intechopen.com

Chapter 5

Charge Separation and Electric Field at a Cylindrical Plasma Edge

Magdi Shoucri

Additional information is available at the end of the chapter

http://dx.doi.org/10.5772/48353

1. Introduction

There are number of physical situations where plasmas neutrality breaks down through boundary layers called plasma sheaths, which are either free or in contact with a wall. The plasma sheaths transition problems are at the heart of an industrial revolution whose theme is the design of matter on the molecular scale.The study of the charge separation at a plasma edge requires generally the solution of the kinetic equations of plasmas which, for a collisionless plasma, usually reduce to the well-known Vlasov equation. Some examples for the solution of the Vlasov equation for sheaths transition problems have been presented in Shoucri, 2008a, 2009a. A problem of interest is the problem involving the generation of radial electric fields and poloidal flows to achieve radial force balance at a steep density gradient in the presence of an external magnetic field. This problem is of great importance in the steep density gradients pedestal of the high confinement mode (H-mode) in tokamaks, since it largely affects the edge physics of the H-mode. In the present work, we shall study the problem of the generation of a charge separation and the associated electric field at the edge of a cylindrical plasma column, in the presence of an external magnetic field directed along the cylinder axis. In previous publications on this problem (Shoucri *et al.*, 2003, 2004, 2008b, 2009b), we have considered the case where the electrons were frozen by the magnetic field lines, with a constant density profile which changes rapidly along the gradient over an ion orbit size. Along the gradient the electrons bound by the magnetic field cannot move across this field to exactly compensate the ion charge which results from the finite ions' gyroradius. This effect is especially important for large values of the ratio ρ_i / λ_{De}, where ρ_i is the ions' gyroradius and λ_{De} is the Debye length. Accurate calculation of the charge separation is important for the accurate calculation of the self-consistent electric field. This requires also an accurate calculation of the exact ion orbits using a kinetic equation. In the present work, we use an Eulerian Vlasov code to study the

evolution of the ion distribution function for the problem of the charge separation at the edge of a cylindrical plasma, in the presence of an external magnetic field directed along the cylinder axis. Eulerian codes have the advantage of a very low noise level and make it possible to measure accurately a very small charge separation (Shoucri *et al.*, 2003, Shoucri *et al.*, 2004 & Shoucri, 2009a,b), and allows accurate results in the low density regions of the phase-space.

It was pointed out in the analysis of H-mode power threshold in a tokamak by Groebner *et al.*, 2001, that the changes in the electron density n_e and ∇n_e in the transition to H-mode are small, and changes in T_e are barely perceptible in the data. Electrons and ions have a density profile which varies rapidly along the gradient over an ion orbit size. In previous publications (Shoucri *et al.*, 2003, 2004, Shoucri, 2002, 2008a,b, 2009a,b) the electrons density and temperature profiles were kept constant. In the present work we will allow the electrons to move, and it will be sufficient for the purpose of our study to describe the motion of the electrons, having a small gyroradius, by a guiding center equation (Shoucri *et al.*, 1997). This allows a more accurate description of the contribution of the electrons, with respect to the approximation previously used in Shoucri *et al.*, 2003, 2004, 2009a, where the profile of the electrons was assumed constant in time. The electrons motion across the magnetic field in the gradient region is limited by the guiding center equation, and the magnetized electrons cannot move sufficiently across the magnetic field to compensate the charge separation which results from the ions motion due to the finite ion orbits. To determine this charge separation at the plasma edge along the gradient, it is important to calculate the ion orbits accurately by using an Eulerian Vlasov code. The larger the ions' gyroradius, the bigger the charge separation and the self-consistent electric field at the edge. (Hence the important role played by even small fractions of impurity ions, because of their large gyroradii, in enhancing the electric field at the plasma edge).

In full toroidal geometry, there are "neoclassical" effects which can play a role in this problem, such as the neoclassical enhancement of the classical ion polarization drift, or the neoclassical damping of poloidal flows (Stix, 1973, Hirshman 1978, Waltz *et. al.*, 1999). We focus for simplicity in the present work on a cylindrical geometry for the problem of the generation of an electric field and poloidal flow at a plasma edge due to the finite ions' gyroradius, when the external magnetic field is applied along the axis of the cylinder. The solution we present is a two-dimensional (2D) solution in a cylindrical geometry, with the external magnetic field assumed uniform along its axis. We compare the radial electric field calculated along the gradient with the macroscopic values calculated from the kinetic code for the gradient of the ion pressure in the radial direction, and we find that this quantity balances the radial electric field fairly well, a result similar to what has been presented in one-dimensional geometry (Shoucri, 2002, Shoucri *et al*. 2003, 2004). The contribution of the Lorentz force term along the gradient is negligible. For the parameters we use in the present work, the solution allows for a small value of E_θ to exist, especially on the high field side of the cylinder as it will be discussed below, which causes a small oscillation in the radial direction.

As mentioned above, the ions are described by a kinetic Vlasov equation and the electrons are described by a guiding center equation. These equations are solved numerically using a method of characteristics. There have been important advances in the last few decades in the domain of the numerical solution of hyperbolic type partial differential equations using the method of characteristics. The application of the method of characteristics for the numerical solution of the kinetic equations of plasmas and for the guiding center equations has been recently discussed in several publication (see for instance Shoucri, 2008a,c, 2009a). These methods are Eulerian methods which use a computational mesh to discretize the equations on a fixed grid, and have been successfully applied to different important problems in plasma physics involving kinetic equations, such as laser-plasma interaction (Ghizzo *et al*., 1990, 1992, Strozzi *et al*., 2006, Shoucri, 2008d), the calculation of an electric field at a plasma edge (Shoucri, 2002, 2008b, 2009b, Shoucri *et al*., 2000, 2003, 2004), the applications of gyro-kinetic codes to study edge physics problems in plasmas (Manfredi *et al*., 1996, Shoucri, 2001, Shoucri *et al*., 2005, Pohn & Shoucri, 2008) and to collisional plasmas (Batishchev *et al*., 1999). These methods present the great advantage of having a low noise level, and allow accurate results in the low density regions of the phase-space (Shoucri, 2008c). In the applications presented (Shoucri, 2008a,c, 2009a), the computation was usually done on a fixed grid, so no dynamical grid adjustment was necessary, and interpolation was restricted to the use of a cubic spline, which compared favourably with other methods (see, for instance, Pohn *et al*., 2005), so altogether the method was accurate and remained relatively simple. Interpolation in several dimensions using a tensor product of cubic *B*-splines has been also successfully applied (Sonnendrücker *et al*., 1999, Shoucri, 2008a, 2009a, 2011). The method of characteristics has been also successfully applied in fluids to problems having shock wave solution (Shoucri & Shoucri, 2007). Large Courant-Frederichs-Levy (CFL) computation parameter is possible, and therefore the time-step numerical limitation by large velocities can be removed, if the physics makes it possible. A more complete study on splines can be found in the book of Ahlberg *et al*., 1967, and an important theoretical study on the method of characteristics can be found, for instance, in the book of Abbott, 1966. More applications to plasma physics problems can be found in the several references we have cited.

2. The relevant equations and the numerical method

We consider the cylindrical coordinate system (r,θ,z). The plasma is uniform in the z direction. The radial direction in the cylindrical plasma is normal to a vessel surface which is located at $r = r_{max}=R$. The constant magnetic field is in the z direction which represents the toroidal direction, and θ is the poloidal direction. The constant magnetic field in the z direction is given by:

$$\vec{B} = \frac{B_0 \vec{e}_z}{1+\varepsilon\cos\theta} \tag{1}$$

where B_0 is the magnetic field along the axis of the cylinder at $\theta = \pi/2$, and $\varepsilon = r / R_{maj}$ where R_{maj} is the major radius of the tokamak. We assume that at $r = r_{max}=R$ we have R / R_{maj} =0.2. In this case we can also write $\varepsilon = r / R_{maj} = 0.2r / R$. We consider a deuterium plasma,

$m_i / m_e = 2\text{x}1836$. The ions are described by the normalized 2D Vlasov equation for the ions distribution function $f_i(r,\theta,v_r,v_\theta,t)$:

$$\frac{\partial f_i}{\partial t} + v_r \frac{\partial f_i}{\partial r} + \frac{v_\theta}{r}\frac{\partial f_i}{\partial \theta} + \left(E_r + \omega_{ci}\upsilon_\theta + \frac{\upsilon_\theta^2}{r} \right) \frac{\partial f_i}{\partial v_r} + \left(E_\theta - \omega_{ci} v_r - \frac{v_r v_\theta}{r} \right) \frac{\partial f_i}{\partial v_\theta} = 0 \tag{2}$$

where from Eq.(1) the ion cyclotron frequency $\omega_{ci} = \omega_{ci0} / (1 + \varepsilon \cos\theta)$. The electrons are described by the normalized 2D guiding-center equation:

$$\frac{\partial n_e}{\partial t} + \nabla . \vec{V}_d n_e = 0 \tag{3}$$

where the drift velocity $\vec{V}_d = \vec{E}\text{x}\vec{B} / B^2$. Equation (3) can be developed in our 2D system to give the following equation:

$$\frac{\partial n_e}{\partial t} + V_{dr}\frac{\partial n_e}{\partial r} + V_{d\theta}\frac{\partial n_e}{\partial \theta} = -n_e E_\theta \frac{\partial}{\partial r}\frac{1+\varepsilon\cos\theta}{\omega_{ci0}} + n_e E_r \frac{1}{r}\frac{\partial}{\partial \theta}\frac{1+\varepsilon\cos\theta}{\omega_{ci0}} \tag{4}$$

where $V_{dr} = E_\theta \dfrac{1+\varepsilon\cos\theta}{\omega_{ci0}}$; $V_{d\theta} = -\dfrac{E_r}{r}\dfrac{1+\varepsilon\cos\theta}{\omega_{ci0}}$

This system is coupled to Poisson's equation:

$$\frac{1}{r}\frac{\partial}{\partial r}\left(r\frac{\partial \phi}{\partial r}\right) + \frac{1}{r^2}\frac{\partial^2 \phi}{\partial \theta^2} = -(n_i - n_e);\ E_r = -\frac{\partial \phi}{\partial r};\ E_\theta = -\frac{1}{r}\frac{\partial \phi}{\partial \theta} \tag{5}$$

Time is normalized to the inverse plasma frequency ω_{pi}^{-1} , velocity is normalized to the acoustic velocity $C_s = \sqrt{T_e / m_i}$, and length is normalized to the Debye length $\lambda_{De} = C_s / \omega_{pi}$. T_e is the electron temperature and m_i is the ion mass. The potential is normalized to T_e / e , and the electric field is normalized to $T_e / (e\lambda_{De})$, and the density is normalized to the peak initial central density. The ion cyclotron frequency ω_{ci} as previously defined is normalized to ω_{pi} . The system is solved over a length $r_L = 175$ Debye lengths in front of the vessel surface, with an initial ion distribution function for the deuterons over the domain $r = \{R - r_L, R\}$ given in our normalized units, by:

$$f_i(r, \theta, v_r, v_\theta) = n_i(r) \frac{e^{-\left(v_r^2 + v_\theta^2\right)/2\,T_i}}{2\pi T_i} \ ; \tag{6}$$

$n_i(r)$ and $n_e(r)$ are the initial ion and electron density profiles respectively, with $n_e(r) = n_i(r)$ in the initially neutral system. *R* is the radius of the cylinder as we previously mentioned. We also use the following parameters:

$$\frac{T_i}{T_e}=1\,;\quad \frac{\rho_i}{\lambda_{De}}=\sqrt{\frac{2T_i}{T_e}}\frac{1}{\omega_{ci0}/\omega_{pi}}=20 \tag{7}$$

In the present calculations the parameter $\omega_{ci0}/\omega_{pi}=0.1/\sqrt{2}$. With the initial distribution function for the ions in Eq. (6), we have $T_{i\theta}=T_{ir}=T_i$ spatially constant, the factor $2T_i$ in Eq. (7) in the calculation of the gyroradius takes into account the fact that the perpendicular temperature is $\left\langle v_\perp^2\right\rangle=\left\langle v_r^2\right\rangle+\left\langle v_\theta^2\right\rangle=\frac{2T_i}{m_i}$.

Equations (2) and (3) are solved by a method of fractional step (Yanenko, 1971), first applied for a Vlasov equation by Cheng & Knorr, 1976, and Gagné & Shoucri, 1977, coupled to a method of characteristics. For the general case where several dimensions are involved, the fractional step technique allows the reduction of the multi-dimensional equation to an equivalent set of reduced equations. To advance Eq. (2) and Eq.(3) for one time-step Δt, the splitting of the equations is applied as follows.

Step 1. We solve for $\Delta t/2$ the equations:

$$\frac{\partial f_i}{\partial t}+v_r\frac{\partial f_i}{\partial r}+\frac{v_\theta}{r}\frac{\partial f_i}{\partial\theta}=0 \tag{8}$$

$$\frac{\partial n_e}{\partial t}+V_{dr}\frac{\partial n_e}{\partial r}+V_{d\theta}\frac{\partial n_e}{\partial\theta}=0 \tag{9}$$

Equations (8) and (9) are solved by interpolation along their characteristics, to be described below. We then solve Poisson's equation in Eq.(5) to calculate the new electric field.

Step 2. We solve for Δt the equations:

$$\frac{\partial f_i}{\partial t}+\left(E_r+v_\theta\,\omega_{ci}+\frac{v_\theta^2}{r}\right)\frac{\partial f_i}{\partial v_r}+\left(E_\theta-\omega_{ci}\,v_r-\frac{v_r v_\theta}{r}\right)\frac{\partial f_i}{\partial v_\theta}=0 \tag{10}$$

$$\frac{\partial n_e}{\partial t}=-n_e E_\theta\frac{\partial}{\partial r}\frac{1+\varepsilon\cos\theta}{\omega_{ci0}}+n_e E_r\frac{1}{r}\frac{\partial}{\partial\theta}\frac{1+\varepsilon\cos\theta}{\omega_{ci0}} \tag{11}$$

Again Eq.(10) is solved by a method of characteristics, to be described below.

Step 3. We repeat **Step1** for $\Delta t/2$, and then solve Eq.(5) to calculate the new electric field E_r^{n+1}, E_θ^{n+1}.

This completes a one time-step cycle Δt.

2.1. The solution for Step 1

For the solution of Eq. (8), we first solve the characteristic equations:

$$\frac{dr}{dt} = v_r \;; \qquad \frac{d\theta}{dt} = \frac{v_\theta}{r} \tag{12}$$

at a given (v_r, v_θ) in velocity space. The solution of Eqs (12) originating at (r_o, θ_o) at time *t*, and reaching the grid point (r, θ) at $t = t + \Delta t/2$ can be written as follows, for a half time-step $\Delta t/2$:

$$r_o = r - \upsilon_r \Delta t/2; \; \theta_o = \theta - \frac{\upsilon_\theta}{\upsilon_r} \ln \frac{r}{r - \upsilon_r \Delta t/2} \tag{13}$$

For $v_r \, \Delta t/2 \ll 1$, the second equation reduces to $\theta_o = \theta - \frac{v_\theta}{r} \Delta t/2$. Therefore the solution of Eq. (8) can be written, for half a time-step $\Delta t/2$, as follows:

$$f_i^* \left(r, \theta, v_r, v_\theta, t + \Delta t/2\right) = f_i \left(r - v_r \, \Delta t/2, \theta - \frac{v_\theta}{v_r} \ln \frac{r}{r - v_r \Delta t/2}, v_r, v_\theta, t \right) \tag{14}$$

The right hand side of Eq. (14) is calculated by interpolation using a tensor product of cubic *B*-splines, in which θ is periodic (Shoucri *et al.*, 2004, Shoucri, 2008a, 2009a). For each v_r and v_θ, we write for the interpolation function $s(r, \theta)$:

$$s(r, \theta) = \sum_{j=0}^{N_r} \sum_{k=0}^{N_\theta} \eta_{jk} B_j(r) B_k(\theta) \tag{15}$$

taking into account that θ is periodic. $B_j(r)$ and $B_k(\theta)$ are cubic splines.The cubic *B*-spline is defined as:

$$B_j(x) = \frac{1}{6h^3} \begin{cases} (x - x_j)^3 & x_j \le x < x_{j+1} \\ h^3 + 3h^2 (x - x_{j+1}) + 3h(x - x_{j+1})^2 & \\ \qquad - 3(x - x_{j+1})^3 & x_{j+1} \le x < x_{j+2} \\ h^3 + 3h^2 (x_{j+3} - x) + 3h(x_{j+3} - x)^2 & \\ \qquad - 3(x_{j+3} - x)^3 & x_{j+2} \le x < x_{j+3} \\ (x_{j+4} - x)^3 & x_{j+3} \le x < x_{j+4} \end{cases} \tag{16}$$

and $B_j(x) = 0$ otherwise. The grid size *h* (either Δr or $\Delta\theta$ in our notation), is assumed uniform. For the calculation of the coefficients η_{jk} of the cubic *B*-spline interpolation function $s(r, \theta)$ for periodic θ in Eq.(15) see details in Shoucri *et al.*, 2004 and Shoucri, 2008a, 2009a.

We then solve Eq.(9) for a half time-step $\Delta t/2$ along the characteristics:

$$\frac{dr}{dt} = V_{dr}(r, \theta) = E_\theta \frac{1 + \varepsilon \cos\theta}{\omega_{ci0}} \;; \qquad \frac{d\theta}{dt} = V_{d\theta}(r, \theta) = -\frac{E_r}{r} \frac{1 + \varepsilon \cos\theta}{\omega_{ci0}} \tag{17}$$

Equations (17) are solved using an iterative process. We assume that at the time-step $t_{n+1/2} = t_n + \Delta t/2$, r is at the grid point j_r and θ is at the grid point j_θ. The following leapfrog scheme can be written for the solution of Eq.(17):

$$\frac{r_{j_r} - r(t_n)}{\Delta t/2} = V_{dr}(r^{n+1/4}, \theta^{n+1/4}) = V_{dr}(\frac{r_{j_r} + r(t_n)}{2}, \frac{\theta_{j_\theta} + \theta(t_n)}{2}) \tag{18}$$

$$\frac{\theta_{j_\theta} - \theta(t_n)}{\Delta t/2} = V_{d\theta}(r^{n+1/4}, \theta^{n+1/4}) = V_{d\theta}(\frac{r_{j_r} + r(t_n)}{2}, \frac{\theta_{j_\theta} + \theta(t_n)}{2}) \tag{19}$$

where $(r(t_n), \theta(t_n))$ is the point where the characteristic is originating at t_n (not necessarily a grid point). Put:

$$\Delta_r = \frac{r_{j_r} - r(t_n)}{2};\ \Delta_\theta = \frac{\theta_{j_\theta} - \theta(t_n)}{2} \tag{20}$$

we can rewrite Eqs.(18,19) as follows:

$$\Delta_r = \frac{\Delta t}{4} V_{dr}(r_{j_r} - \Delta_r, \theta_{j_\theta} - \Delta_\theta) \tag{21}$$

$$\Delta_\theta = \frac{\Delta t}{4} V_{d\theta}(r_{j_r} - \Delta_r, \theta_{j_\theta} - \Delta_\theta) \tag{22}$$

which are implicit equations for $(\Delta_r, \Delta_\theta)$, and which are solved by iteration. Usually, two iterations are sufficient for convergence. We start with $(\Delta_r^0 = 0, \Delta_\theta^0 = 0)$. We get at the first iteration:

$$\Delta_r^1 = \frac{\Delta t}{4} V_{dr}(r_{j_r}, \theta_{j_\theta}) = \frac{\Delta t}{4} E_\theta(r_{j_r}, \theta_{j_\theta}) \frac{1 + \frac{r_{j_r}}{R}\cos\theta_{j_\theta}}{\omega_{ci0}} \tag{23}$$

$$\Delta_\theta^1 = \frac{\Delta t}{4} V_{d\theta}(r_{j_r}, \theta_{j_\theta}) = -\frac{\Delta t}{4} \frac{E_r(r_{j_r}, \theta_{j_\theta})}{r_{j_r}} \frac{1 + \frac{r_{j_r}}{R}\cos\theta_{j_\theta}}{\omega_{ci0}} \tag{24}$$

Second iteration:

$$\Delta_r^2 = \frac{\Delta t}{4} V_{dr}(r_{j_r} - \Delta_r^1, \theta_{j_\theta} - \Delta_\theta^1) = \frac{\Delta t}{4} E_\theta(r_{j_r} - \Delta_r^1, \theta_{j_\theta} - \Delta_\theta^1) \frac{1 + \frac{r_{j_r} - \Delta_r^1}{R}\cos(\theta_{j_\theta} - \Delta_\theta^1)}{\omega_{ci0}} \tag{25}$$

$$\Delta_\theta^2 = \frac{\Delta t}{4} V_{d\theta}(r_{j_r} - \Delta_r^1, \theta_{j_\theta} - \Delta_\theta^1) = -\frac{\Delta t}{4} \frac{E_r(r_{j_r} - \Delta_r^1, \theta_{j_\theta} - \Delta_\theta^1)}{r_{j_r} - \Delta_r^1} \frac{1 + \frac{r_{j_r} - \Delta_r^1}{R} \cos(\theta_{j_\theta} - \Delta_\theta^1)}{\omega_{ci0}} \tag{26}$$

The quantities $E_r(r_{j_r} - \Delta_r^1, \theta_{j_\theta} - \Delta_\theta^1)$ and $E_\theta(r_{j_r} - \Delta_r^1, \theta_{j_\theta} - \Delta_\theta^1)$ are calculated by a cubic *B*-spline interpolation, similar to what is described in Eq.(15). Finally to advance Eq.(9) by $\Delta t / 2$, we calculate:

$$n_e^*(r_{j_r}, \theta_{j_\theta}, t + \Delta t / 2) = n_e(r_{j_r} - 2\Delta_r^2, \theta_{j_\theta} - 2\Delta_\theta^2, t) \tag{27}$$

where the right hand side of Eq.(27) is calculated again using a cubic *B*-spline interpolation as indicated in Eq.(15).

2.2. The solution for Step 2

We go to **Step2** and solve for Δt Eqs.(10,11). We first solve the equation:

$$\frac{\partial f_i}{\partial t} + \left(E_r + \omega_{ci} \upsilon_\theta + \frac{\upsilon_\theta^2}{r} \right) \frac{\partial f_i}{\partial v_r} + \left(E_\theta - \omega_{ci} v_r - \frac{v_r v_\theta}{r} \right) \frac{\partial f_i}{\partial v_\theta} = 0 \tag{28}$$

The electric field E_θ remained small, since $E_\theta = -\frac{1}{r} \frac{\partial \phi}{\partial \theta}$, and $r \sim R$ =5000 towards the edge in our calculation.

$$\frac{dv_r}{dt} = E_r + v_\theta \omega_{ci} + \frac{v_\theta^2}{r}; \qquad \frac{dv_\theta}{dt} = E_\theta - \omega_{ci} v_r - \frac{v_r v_\theta}{r} \tag{29}$$

Following the same iterative steps as described for Eq.(27), to an order $O(\Delta t)^2$ the solution of Eq. (29) yields the following solution to Eq.(28):

$$f_i^{**}(r, \theta, v_r, v_\theta, t + \Delta t) = f_i^*(r, \theta, v_r - 2a, v_\theta - 2b, t) \tag{30}$$

Again the 2D interpolation in Eq. (30) is done using a tensor product of cubic *B*-spline, as explained in Eq.(15), and *a* and *b* are calculated with similar iterative steps as in Eqs.(23-26) and are given, to an order $O(\Delta t)^2$, by the expressions:

$$a = \frac{\Delta t}{2} \left\{ E_r + \omega_{ci} \left(v_\theta - b^1 \right) + \frac{(\upsilon_\theta - b^1)^2}{r} \right\} \tag{31}$$

$$b = \frac{\Delta t}{2} \left\{ E_\theta - \omega_{ci} \left(v_r - a^1 \right) - \frac{(\upsilon_\theta - b^1)(\upsilon_r - a^1)}{r} \right\} \tag{32}$$

where $a^1 = \frac{\Delta t}{2}\left\{E_r + \omega_{ci}\upsilon_\theta + \frac{\upsilon_\theta^2}{r}\right\};\ b^1 = \frac{\Delta t}{2}\left\{E_\theta - \omega_{ci}\upsilon_r - \frac{\upsilon_\theta\upsilon_r}{r}\right\}$

The density $n_e^{**}(r,\theta,t+\Delta t)$ is calculated by integrating Eq.(11) as follows:

$$n_e^{**}(r,\theta,t+\Delta t) = n_e^{*}\exp(-E_\theta\frac{\partial}{\partial r}\frac{1+\frac{r}{R}\cos\theta}{\omega_{ci0}}\Delta t + E_r\frac{1}{r}\frac{\partial}{\partial\theta}\frac{1+\frac{r}{R}\cos\theta}{\omega_{ci0}}\Delta t) \tag{33}$$

where n_e^* is calculated in Eq.(27). To calculate f_i^{n+1} and n_e^{n+1}, we then repeat **Step 1** for the solution of Eqs. (8,9) for $\Delta t/2$ using f_i^{**} and n_e^{**} calculated from Eq.(30) and Eq.(33). The electric field is then updated to calculate $E_r^{n+1}(r,\theta)$ and $E_\theta^{n+1}(r,\theta)$ by solving Poisson equation.

2.3. The solution of Poisson's equation

Equation (5) is solved by first Fourier transforming the equation in the periodic direction θ:

$$\phi(r,\theta) = \sum_m \phi_m(r)e^{im\theta} \tag{34}$$

and the resulting equation is then discretized in the radial direction over a uniform grid following the method of Knorr *et al.*, 1980 (also rediscussed more recently in Crouseilles *et al.* 2009):

$$-A_m\phi_{m,j+1} + B_m\phi_{m,j} - C_m\phi_{m,j-1} = \frac{(\Delta r)^2}{12}(\rho_{m,j+1} + 10\rho_{m,j} + \rho_{m,j-1}) \tag{35}$$

where

$$A_{m,j} = 1 + \frac{\Delta r}{2r_j} - \frac{m^2(\Delta r)^2}{12r_j^2};\ B_{m,j} = 2 + \frac{10m^2(\Delta r)^2}{12r_j^2};\ C_{m,j} = 1 - \frac{\Delta r}{2r_j} - \frac{m^2(\Delta r)^2}{12r_j^2} \tag{36}$$

and $\phi_{m,j} = \phi_m(r_j)$; $\rho = n_i - n_e$; $n_i = \iint f_i(r,\theta,v_r,v_\theta)dv_r dv_\theta$

Equation (35) is solved using a tridiagonal algorithm. To get the boundary conditions, we assume in the present calculation that the deuterons and electrons currents hitting the cylindrical wall surface at $r = R$ are collected by a floating potential cylindrical vessel. Therefore we have the relations for the charge collected:

$$\left.\frac{\partial E_r(r,\theta)}{\partial t}\right|_{r=R} = -(J_{ri}\big|_{r=R} - J_{re}\big|_{r=R}) \quad \text{or} \quad E_r(r,\theta)\big|_{r=R} = -\int_0^t (J_{ri}\big|_{r=R} - J_{re}\big|_{r=R})dt \tag{37}$$

where

$$J_{ri}(r,\theta) = \int v_r f_i\left(r,\theta,v_r,v_\theta,t\right) dv_\theta dv_r \quad ; \qquad J_{re} = n_e V_{dr} \tag{38}$$

and V_{dr} is defined in Eq.(17). $E_r\big|_{r=R} \equiv E_r\big|_R$ from Eq.(37) is used to obtain for the potential the following boundary condition at $r = R$:

$$E_r\big|_R = -\frac{\partial\phi}{\partial r}\bigg|_R \tag{39}$$

By integrating the relation $\nabla.\vec{E} = \rho$, we get a relation between the charge collected on the cylindrical wall and the charge appearing in the initially neutral plasma:

$$R\,E_r\big|_R - (R - r_L)\,E_r\big|_{R-r_L} + \int_{R-r_L}^{R} \frac{\partial E_\theta}{\partial\theta} dr = \sigma; \text{ where } \sigma = \int_{R-r_L}^{R} \rho r dr \tag{40}$$

where r_L is the width of the plasma slab, which extends from $R - r_L$ to R at the edge of the cylindrical plasma of radius R. σ is the charge appearing in the system. From Eq.(40), we get the following relation:

$$E_r\big|_{R-r_L} = -\frac{\partial\phi}{\partial r}\bigg|_{R-r_L} = (R\,E_r\big|_R - (\sigma - \int_{R-r_L}^{R} \frac{\partial E_\theta}{\partial\theta} dr)) / (R - r_L) \tag{41}$$

We assume that the plasma particles are allowed to enter or leave at the boundary at $r = R - r_L$. So the difference between the electric fields at the boundary $r = R - r_L$ and at $r = R$ must be such that Eq. (40) must be satisfied at every time-step in every direction θ. In the present simulation, $E_r\big|_{r=R}$ is calculated from Eq. (37), which defines the derivative of the potential at the right boundary to be used in the solution of Eq. (35). We fix the potential to be zero at the boundary at $r = R - r_L$ and solve Poisson equation in Eq.(35) for the potential. Then the resulting electric field at $E_r\big|_{r=R-r_L}$, calculated at $r = R - r_L$ from Eq. (5), must satisfy Eq. (41).

The initial density profiles at the neutral plasma edge are given by:

$$n_i(r) = n_e(r) = 0.5(1 + \tanh((R - r - 2r_L / 5) / 4)) \tag{42}$$

The profiles in Eq. (42) situate the steep gradient to be centered at a distance of $2r_L / 5$ from the wall of the vessel, which put the plasma relatively close to the floating wall of the vessel. The wall of the vessel will collect the charge coming from the plasma, especially due to the large ions gyroradius. The system is solved for an edge thickness $r_L = 175$, and R=5000 for the radius of the cylinder (we expect this radius to be large in a tokamak, so in the domain $r = (R - r_L, R)$, the variation of the quantity r / R remains very close to 1.

We use N=250 grid points in space in the radial direction, and 128 grid points in the azimuthal direction. 80 grid points are used in each velocity direction. The velocity extrema for the ions velocities are $\pm 4\sqrt{T_e / T_i}$ in our normalized units, with T_e/T_i =1 in the present simulations.

3. Results

The code was executed for a sufficiently long time to reach a steady state. We noted around t=500 that the code has indeed reach a steady state. Since $\omega_{ci0} = 0.1/\sqrt{2}$ (normalized to ω_{pi}), then the gyroperiod $\tau = 2\pi/\omega_{ci0} \approx 88$. This means that the code has executed more than 5 gyroperiods. Figure(1) shows the electric field at $\theta = 0$ (full curve), $\theta = \pi/2$ (broken curve) and $\theta = \pi$ (dashed-dotted curve), at time t = 495 (left figure) and t=500 (right figure). At the edge and along the gradient the electric field E_r is directed towards the center to the interior of the plasma. The electric field at the floating vessel wall at $r = R$ was calculated using Eq. (37) at 128 points over the 2π circle. We see from Fig. (1) that the electric field at $\theta = 0$ is higher (in absolute value) than the one at $\theta = \pi$, and we note that the curves for $0<R-r<75$ have reached a steady state stable equilibrium, with the charge collected at $r=R$ remaining constant, while towards the center for $75<R-r<175$, the curve at $\theta = \pi$ shows a small steady state oscillation around zero. The charge collected on the floating wall of the cylindrical vessel at $\theta = 0,\ \pi/2$ and π are respectively -0.1455, -0.1389 and -0.063 at t=500. For the solution of Poisson equation, we set the value of the electric field $E_r\big|_{r=R}$ at the cylindrical vessel wall exactly equal to the charge collected on the wall according to Eq.(37). If the charge collected on the wall is equal to the charge appearing in the system, then according to Eq.(41) :

$$E_r\big|_R \approx (\sigma - \int_{R-r_L}^{R} \frac{\partial E_\theta}{\partial \theta} dr))/R \quad ; \qquad E_r\big|_{R-r_L} \approx 0 \tag{43}$$

which is what we see for the curves at $\theta = 0$ and $\pi/2$ in Fig.(1). Indeed the code calculate for the charge appearing in the system $(\sigma - \int_{R-r_L}^{R} \frac{\partial E_\theta}{\partial \theta} dr))/R$ the values of -0.1475 and -0.1399, very close to the values of -0.1455 and -0.1389 calculated for $E_r\big|_R$ at $\theta = 0$ and $\pi/2$ as we previously mentioned. And the quantity $E_r\big|_{R-r_L}$ was negligible by an order of magnitude ($2.\text{x}10^{-3}$ and $1.\text{x}10^{-3}$ at $\theta = 0$ and $\pi/2$ respectively).

In our code, we allow at $r = R - r_L$ for the possibility of plasma to flow across the boundary. Note that for our present set of the parameters the electric field E_θ calculated remained negligible from $\theta = 0$ to $\pi/2$ (see Fig.(6) below), and small around $\theta = \pi$.

Around $\theta = \pi$, the charge appearing in the system is not exactly equal to the charge collected at the cylindrical vessel wall, but shows a small oscillation due the fact that there is a small plasma circulation at $r = R - r_L$. In this case the electric field $E_r\big|_{r=R-r_L}$ is calculated from Eq.(41). At t=500, the value calculated for the right hand side of Eq.(41) is $-1.144\text{x}10^{-2}$, while the value calculated by the code is $-1.155\text{x}10^{-2}$ (which is the value we see in the right figure in Fig.(1) for the $\theta = \pi$ curve). The agreement is very good.

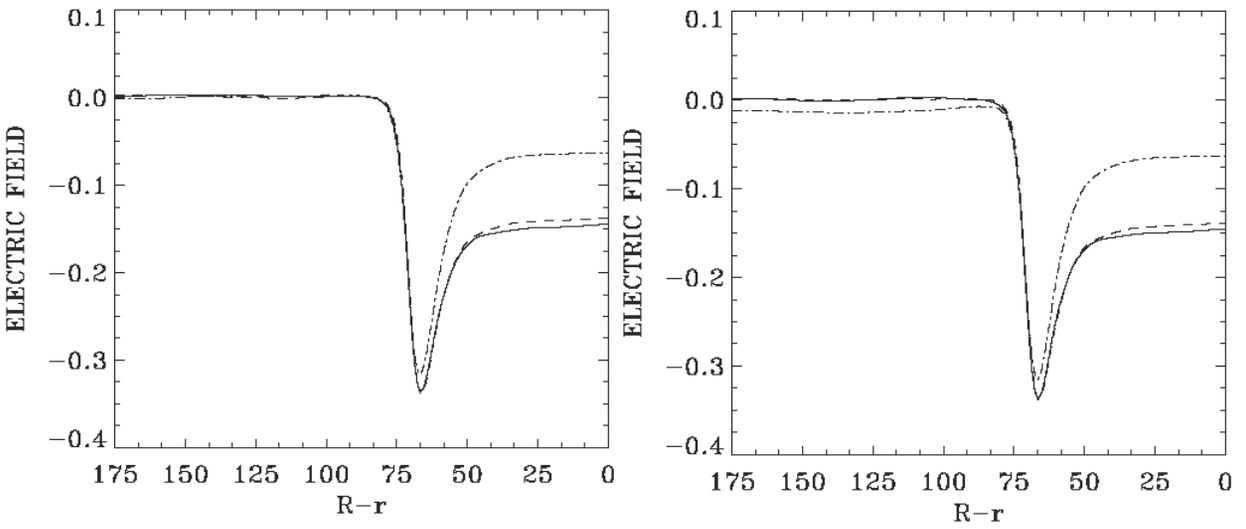

Figure 1. Electric field E_r at $\theta = 0$ (full curve), $\theta = \pi / 2$ (broken curve), and $\theta = \pi$ (dashed-dotted curve), at t=495 (left figure) and t=500 (right figure).

Figure(2) shows the potential at $\theta = 0$ (full curve), $\theta = \pi/2$ (broken line) and $\theta = \pi$ (dashed-dotted line), at time t = 495 (left figue) and t=500 (right figure). The curves at $\theta = 0$ and $\theta = \pi/2$ show negligible oscillation, while the curve at $\theta = \pi$ shows a small oscillation. Since as indicated in Fig.(1) the E_r profiles are essentially constant, especially for $0<R-r<75$ along the gradient, then the oscillation of the curves at $\theta = \pi$ (dashed-dotted line) is taking place in such a way that the slope of the potential $\frac{\partial \phi}{\partial r} = -E_r$ remains constant for $0<R-r<75$. Only for $75<R-r<175$ does the small oscillation of the curve at $\theta = \pi$ in Fig.(2) (dashed-dotted line) translates into a small oscillation of the electric field E_r..

Figure(3) gives at time t = 500 and for $\theta = 0$ the electric field E_r (full curve). Also at $\theta = 0$ the dashed-dotted curve in Fig.(2) gives the Lorentz force, which in our normalized units is given by $-<v_\theta>\omega_{ci}/\omega_{pi} = -\frac{0.1}{\sqrt{2}}<v_\theta>/(1.+0.2\frac{r}{R}\cos\theta)$, and the broken curve gives the pressure force $\nabla P_i / n_i$, $P_i = 0.5\, n_i\left(T_{ir} + T_{i\theta}\right)$, with the following definition:

$$T_{ir,\theta}(r,\theta) = \frac{1}{n_i}\int dv_r\, dv_\theta\, (v_{r,\theta} - < v_{r,\theta} >)^2\, f_i\left(r,\theta, v_r, v_\theta\right) \tag{44}$$

$$< v_{r,\theta} >= \frac{1}{n_i}\int dv_r\, dv_\theta\, v_{r,\theta}\, f_i\left(r,\theta, v_r, v_\theta\right)\ ; \qquad n_i(r,\theta) = \int dv_r\, dv_\theta\, f_i\left(r,\theta, v_r, v_\theta\right) \tag{45}$$

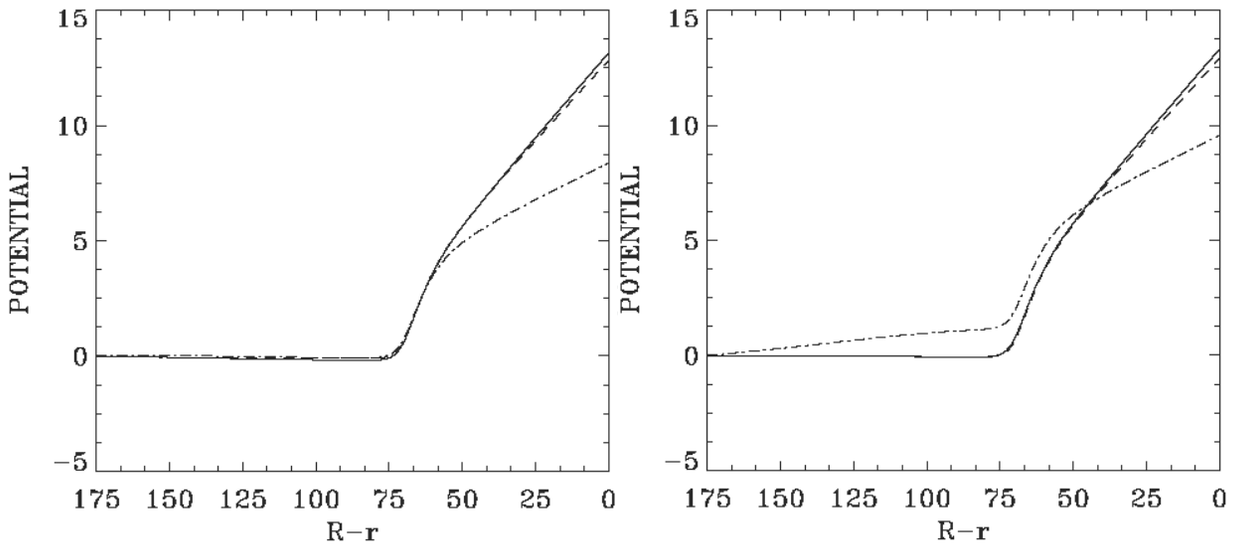

Figure 2. Potential at $\theta = 0$ (full curve), $\theta = \pi / 2$ (broken curve) and $\theta = \pi$ (dashed-dotted curve) at *t*=495 (left gigure) and *t*=500 (right figure).

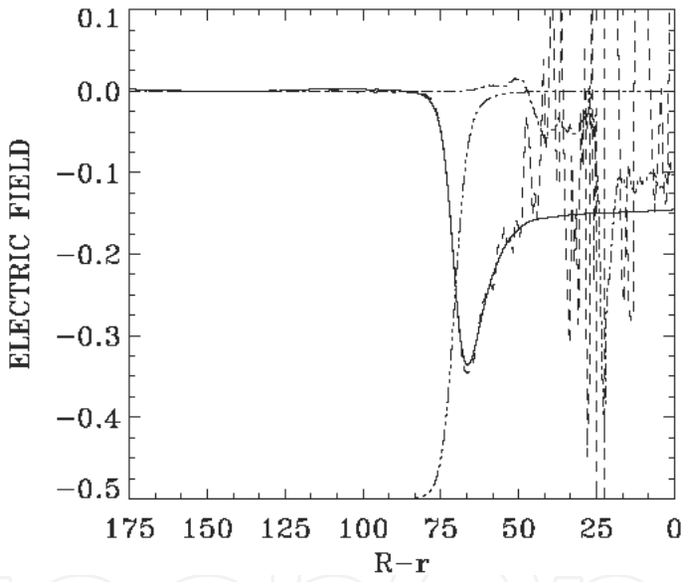

Figure 3. Plot at $\theta = 0$ of the electric field E_r (full curve), the Lorentz force $-(0.1/\sqrt{2}) < v_\theta > /(1. + 0.2(r/R)\cos\theta)$ (dashed-dotted. curve), and the pressure force $\nabla P_i / n_i$ (broken curve). The curve -n_i/2 is plotted for reference (dashed- 3 dotted curve). At time *t* =500.

The $\nabla P_i / n_i$ term (broken curve) shows a very good agreement along the gradient with the solid curve for E_r , and the Lorentz force appears negligible along the gradient. In a region of about two gyroradii from the wall (around 40 Debye lengths from the wall), we have small irregular oscillations in space (and time), the accuracy of $\nabla P_i / n_i$ being degraded by the division with a very small value of the density n_i appearing close to the vessel surface. To avoid this problem, we plot in Fig. (4) the quantities $-(0.1/\sqrt{2}) n_i < v_\theta > /(1. + 0.2(r/R)\cos\theta)$, $n_i E_r, \nabla P_i,$ at $\theta = 0$ (note that $J_{\theta i} = n_i < v_\theta >$). We see that there is a very nice agreement for

the relation $n_i E_r \approx \nabla P_i$ along the gradient (the density $-n_i/10$ is also plotted in Fig.(4) to locate the different profiles with respect to the gradient). The Lorentz force term remains negligible in the gradient region, and remains very small in the bulk at 75<*R*-*r*<175. The $\nabla P_i / n_i$ term is zero in the bulk since n_i and T_i are essentially flat in that region. We have seen in this case that the total charge $(\sigma - \int_{R-r_L}^{R} \frac{\partial E_\theta}{\partial \theta} dr))/R$ appearing in the system and calculated by the code by integrating the charge as in Eq. (40) and by calculating E_θ from Poisson equation, is essentially equal to the electric field $E_r\big|_{r=R}$. We note that curves similar to Fig.(4) can be calculated at different angles θ, showing $n_i E_r$ essentially balanced by the ∇P_i.

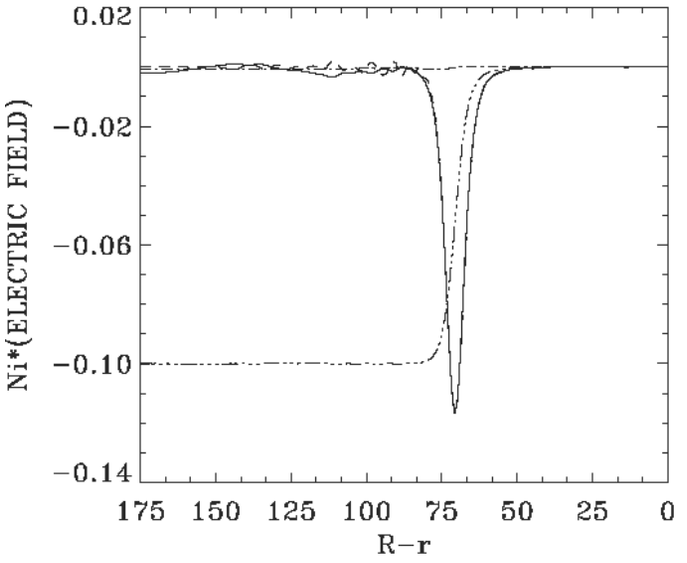

Figure 4. Plot at $\theta = 0$ of $n_i E_r$ (solid curve), $-(0.1/\sqrt{2}) n_i < v_\theta > /(1. + 0.2(r/R)\cos\theta)$ (dash-dot curve), and ∇P_i (broken-curve). The curve –*ni*/10 is plotted for reference (dashed-3 dotted curve). At time *t*=500.

The initial density profiles are given in Eq.(42), so the initial charge is zero. Fig.(5) shows the charge density $n_i - n_e$ at the time $t = 500$ and $\theta = 0$ (full curve), $\theta = \pi/2$ (broken curve) and $\theta = \pi$ (dashed-dotted curve). It is interesting to note that the code was able to maintain the steep density gradients (see Fig.(4) for a plot of n_i). The stable in time steep density profile changes in space rapidly along the gradient over an ion orbit size ($\rho_i / \lambda_{De} = 20$), and the relaxation of the steep gradients during the simulation determines the charge density $n_i - n_e$. The charge density is important along the gradient at the plasma edge. The electrons, described by the guiding center equation given in Eq.(3) cannot compensate along the gradient the charge separation caused by the finite ion gyroradius, which results in the charge density we see in Fig.(5).

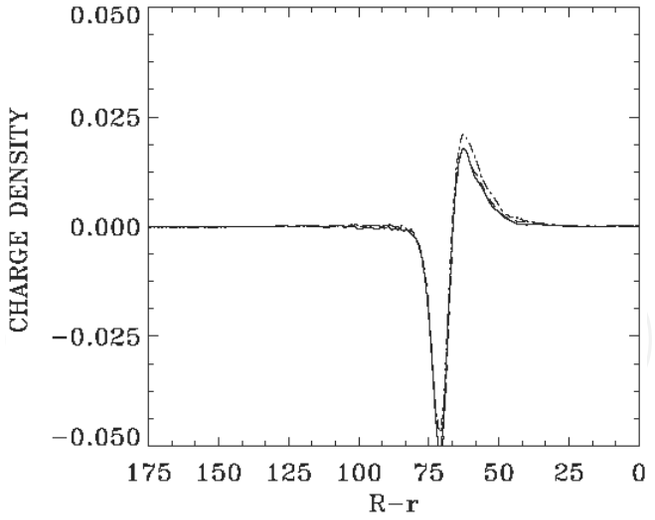

Figure 5. Charge density at $\theta = 0$ (full curve), $\theta = \pi / 2$ (broken curve) and $\theta = \pi$ (dashed-dotted curve), at *t*=500.

We have noted in Fig.(1) the constant value of the E_r profiles, especially for 0<*R-r*<75 along the gradient, translates the constant slope of the potential. However, the potential profile at $\theta = \pi$, although keeping essentially the same slope for 0<*R-r*<75, shows an oscillation in time. This results in a θ variation with an electric field $E_\theta = -\frac{1}{r}\frac{\partial \phi}{\partial \theta}$ which, as we mentioned before, is small for the parameters we are using. Figures (6) presents this electric field E_θ at *t*=485 and *t*=495. It shows no oscillation E_θ in at $\theta = 0$ (full curve, essentially equal to zero), a negligible oscillation at $\theta = \pi/2$ (broken curve), and a small oscillation for the $\theta = \pi$ (dashed-dotted curve), on the high field side of the cylinder. The curve at $\theta = \pi$ is interesting, it shows the oscillating curve for E_θ having a constant flat value in the gradient region, and a linear variation in the inner region.

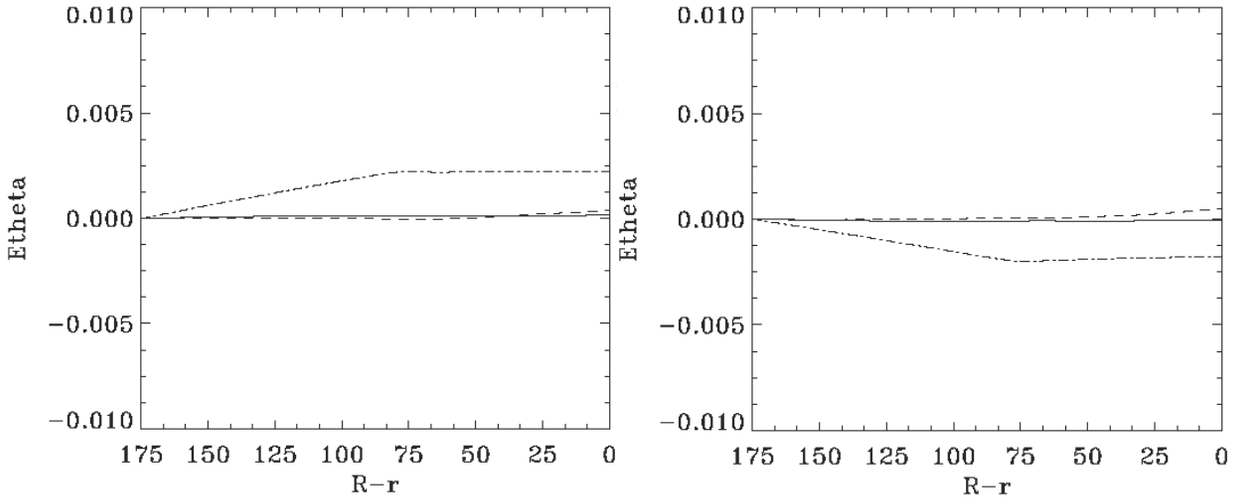

Figure 6. Electric field E_θ at $\theta = 0$ (full curve), $\theta = \pi / 2$ (broken curve), and $\theta = \pi$ (dash-dot curve), at *t*=485 (left figure) and *t*=495 (right figure).

Figure (7) gives at $t = 500$ the temperature T_{ir} as defined in Eq. (43), for $\theta = 0$ (full curve), $\theta = \pi/2$ (broken curve) and $\theta = \pi$ (dashed-dotted curve). The dashed-3 dotted curve is for $n_i T_{ir}$, which is essentially the same for all angles θ. Figure (8) presents similar results for $T_{i\theta}$ as defined in Eq.(43). Note in Fig.(7) and Fig.(8) the division by the very small density at the edge gives irregular oscillations. However the dashed-3 dotted curve in Fig.(7) and Fig.(8) is very smooth, and is for $n_i T_{ir}$ and $n_i T_{i\theta}$ respectively, which removes the problem of the division by the very small density at the edge. We present in Fig.(9) the total pressure $P_i = 0.5\, n_i \left(T_{ir} + T_{i\theta}\right)$ for $\theta = 0$ (full curve), $\theta = \pi/2$ (broken curve) and $\theta = \pi$ (dashed-dotted curve). We see that these curves are essentially identical, for the parameters we are using in the present simulation there is no variation in θ for the total pressure term.

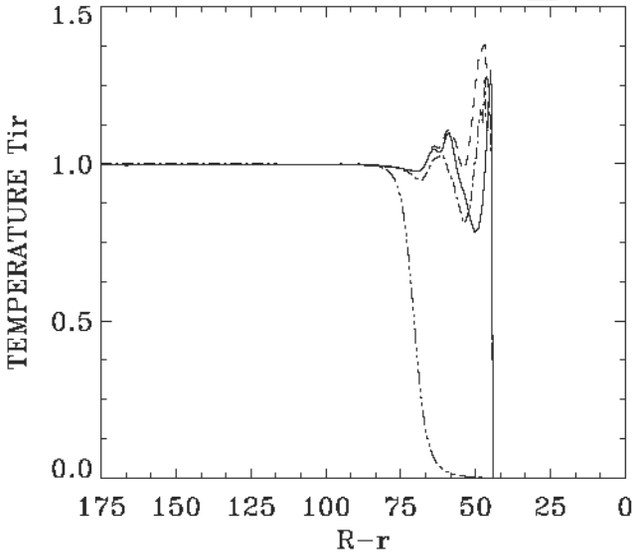

Figure 7. Temperature T_{ir} at $\theta = 0$ (full curve), $\theta = \pi / 2$ (broken curve) and $\theta = \pi$ (dashed-dotted curve). The dashed -3 dotted curve is for $n_i T_{ir}$, which is essentially the same for all θ. Time t=500.

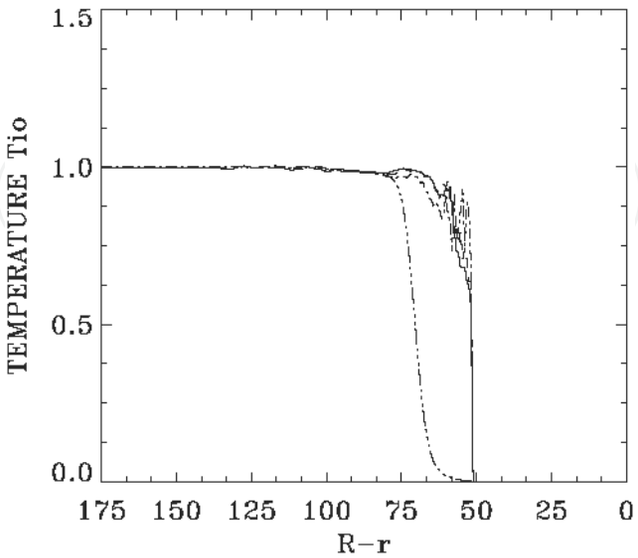

Figure 8. Temperature $T_{i\theta}$ at $\theta = 0$ (full curve), $\theta = \pi / 2$ (broken curve) and $\theta = \pi$ (dash-dot curve). The dashed-3 dotted curve is for $n_i T_{i\theta}$, which is essentially the same for all θ. Time t=500.

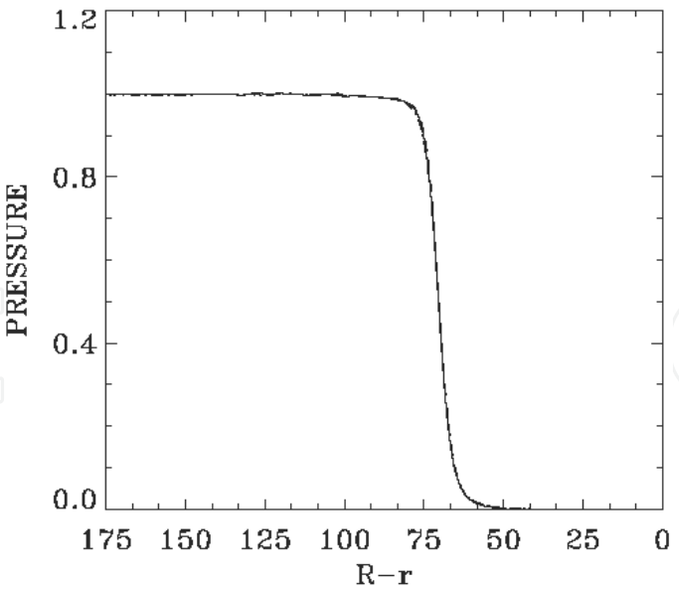

Figure 9. Pressure $P_i = 0.5\, n_i \left(T_{ir} + T_{i\theta}\right)$ at $\theta = 0$ (full curve), $\theta = \pi / 2$ (broken curve) and $\theta = \pi$ (dashed-dotted curve), at *t*= 500.

Figure(10) presents the plot of the θ component of the $\vec{E} \times \vec{B} / B^2$ drift, which in our normalized units is written $-E_r \left(1 + 0.2(r / R)\cos\theta\right)\sqrt{2} / 0.1$, at $\theta = 0$ (full curve), $\theta = \pi/2$ (broken curve) and $\theta = \pi$ (dashed-dotted curve). The curves for 0<*R-r*<75 have reached a stable equilibrium as discussed in Fig.(1) for E_r, while towards the center for 75<*R-r*<175 the curves at $\theta = \pi$ shows a small steady state oscillation around zero, as previously mentioned for E_r in the right figure in Fig.(1). Note in Fig. (10) that this azimuthal (*i.e.* poloidal) $\vec{E} \times \vec{B} / B^2$ drift is flat close to the edge, and is below the acoustic speed at $\theta = \pi$ at the edge, and above the acoustic speed at $\theta = 0$ and $\theta = \pi/2$ at the edge (velocities are normalized to the acoustic speed C_s). We plot in Fig. (11) the total poloidal current (in the θ direction) $n_i \left(\vec{E} \times \vec{B} / B^2 + \vec{v}_D\right)$, where the diamagnetic drift is $\vec{v}_D = \vec{B} \times \nabla n_i T_i / \left(n_i e B^2\right)$. We see that the total current is essentially zero, *i.e.* the profile is adjusting itself so that the $\vec{E} \times \vec{B} / B^2$ drift and the diamagnetic drift are essentially equal and opposite (in our units, the total poloidal current is $\left(-n_i E_r + \nabla p_i\right)\left(1 + 0.2(r / R)\cos\theta\right)\sqrt{2} / 0.1$, essentially equal to zero , showing a small oscillation around zero in Fig.(11), at the left boundary). So the $\vec{E} \times \vec{B} / B^2$ drift is balanced fairly well by the diamagnetic drift. This is the result we get if we calculate the poloidal current:

$$J_{\theta i}(r,\theta) = \int v_\theta f_i\left(r,\theta,v_r,v_\theta,t\right) dv_\theta dv_r \tag{46}$$

We get indeed a negligible value for $J_{\theta i}$. (note that $J_{\theta i} = n_i < v_\theta >$).

We note that due to the small E_θ field (see Fig.6), the $\vec{E} \times \vec{B} / B^2$ drift has a small oscillating component $E_\theta \ (1 + 0.2(r / R)\cos\theta)$ in the radial direction, with a curve similar to what is

presented in Fig.(6). This radial oscillation is negligible around $\theta = 0$ and $\theta = \pi / 2$, and is small on the high field side around $\theta = \pi$, as previously discussed for E_θ in Fig.(6).

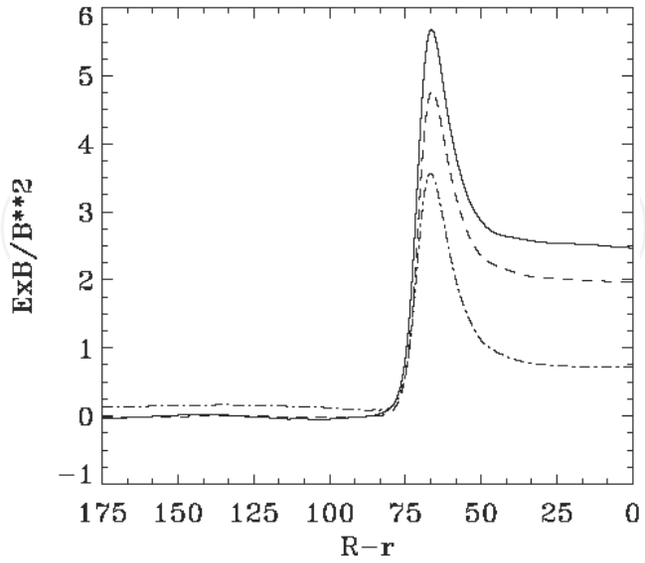

Figure 10. Plot of $-E_r \left(1 + 0.2(r / R)\cos\theta\right)\sqrt{2} / 0.1$ for $\theta = 0$ (full curve), $\theta = \pi / 2$ (broken curve) and $\theta = \pi$ (dashed-dotted curve). At time *t*=500.

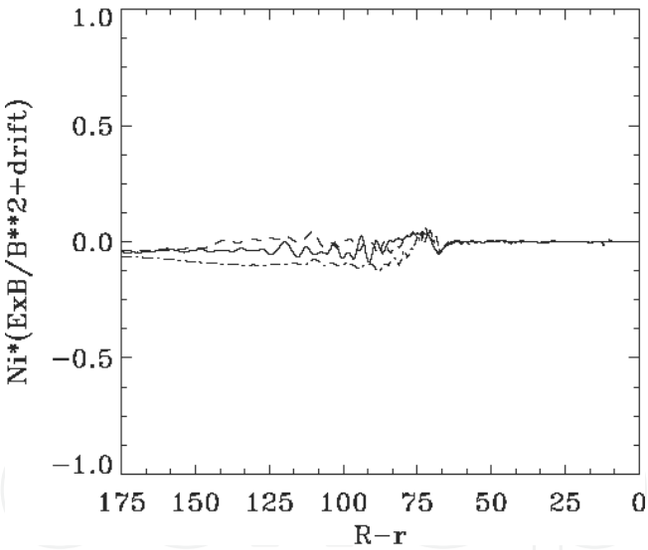

Figure 11. Plot of the total poloidal current $\left(-n_i E_r + \nabla P_i\right) \left(1 + 0.2\,(r / R)\cos\theta\right)\sqrt{2} / 0.1$ for $\theta = 0$ (full curve), $\theta = \pi / 2$ (broken curve) and $\theta = \pi$ (dashed-dotted curve). At time *t*=500.

4. Conclusion

We have presented in this work the self-consistent kinetic solution for the problem of the generation of a charge separation and an electric field at a plasma edge, under the combined effect of a large ratio of the ions' gyroradius to the Debye length ρ_i / λ_{De} (equal to 20 in the simulation we have presented) and a steep density gradient, when the electrons which are

bound to the magnetic field cannot compensate along the gradient the charge separation due to the finite ions' gyroradius. In the cylindrical geometry considered, a fully kinetic equation has been used to describe the ions, and a guiding center equation has been used to describe the electrons bound to the magnetic field. These equations have been solved using the method of characteristics (Shoucri, 2008a,b,c,d, 2009a). The numerical method used for the solution in cylindrical geometry, based on an integration of the equations along the characteristics coupled to a two-dimensional interpolation (Shoucri *et al*., 2004) applied successively in configuration space and in velocity space, is producing accurate results.

The problem of the formation of a charge separation is of great importance in the study of the H-mode physics in tokamaks. We have considered the case where the gradient in the density profiles is located in front of a floating cylindrical vessel. So the charge appearing in the system is essentially equal to the charge collected on the walls of the floating vessel. The solution shows in the radial direction that the electric field along the gradient is balanced by the radial gradient of the pressure, and the total poloidal current is essentially zero. The present results where electrons are described by a guiding center equation are close to what has been previously reported when assuming the electrons stationary and frozen by the magnetic field, and the code shows that a solution with a steep gradient, maintaining a charge separation, where the electron and ion densities vary rapidly over an ion gyroradius, is possible. Also the calculation with the present set of parameters which allow a small value of the poloidal field E_θ to exist, shows the presence of a small oscillation of E_θ on the high field side around $\theta = \pi$ (see Fig.(6)), to which is associated a small radial oscillation due to the radial component of the $\vec{E} \times \vec{B} / B^2$ drift , equal to $E_\theta \left(1 + 0.2\,(r/R)\cos\theta\right)\sqrt{2}/0.1$ in our normalized units.

The present code is a step closer to a code which will include "neoclassical" effects due to toroidal geometry, which can play a role in this problem, such as the neoclassical enhancement of the classical ion polarization drift, or the neoclassical damping of poloidal flows (Stix, 1973, Hirshman 1978, Waltz *et. al.*, 1999).

Author details

Magdi Shoucri
Institut de Recherche Hydro-Québec (IREQ), Varennes, Québec, Canada

Acknowledgement

The author is grateful to Dr. Rejean Girard for his support, and to the Centre de calcul scientifique de l'IREQ (CASIR) for computer time for the simulations presented in this work.

5. References

Abbott, B.A. (1966). *An Introduction to the Method of Characteristics*; Thames and Hudson, London.

Ahlberg, J.H., Nilson, E.N. & Walsh, J.L. (1967). *The Theory of Splines and their Applications*; Academic Press, New York, N.Y.

Batishchev, O., Shoucri, M., Batishcheva, A. & Shkarofsky, I. (1999). Fully Kinetic Simulation of Coupled Plasmas and Neutral Particles in Scrape-off Layer Plasmas of Fusion Devices. *J. Plasma Physics*, Vol. 61, pp. 347- 364

Cheng, C.Z. & Knorr, G. (1976). The Integration of the Vlasov Equation in Configuration Space. *J. Comp. Phys*., Vol. 22, pp. 330-351

Crouseilles, N., Respaud, T. & Sonnendrücker, E. (2009). A Forward Semi-Lagrangian Method for the Numerical Solution of the Vlasov Equation. *Comp. Phys. Comm*., Vol. 180, pp.1730-1745

Gagné, R. & Shoucri, M. (1977). A Splitting Scheme for the Solution of a One-Dimensional Vlasov Equations. *J. Comp. Phys.*, Vol. 24, pp. 445-449

Ghizzo, A., Bertrand, P., Shoucri, M., Johnston, T., Feix M. & Fijalkow, E. (1990). A Vlasov Code for the Numerical Simulation of Stimulated Raman Scattering. *J. Comp. Phys*., Vol. 90, pp. 431-457

Ghizzo, A., Bertrand, P., Shoucri, M., Johnston, T., Fijalkow, E., Feix M. & Demchenko, V.V. (1992). Study of Laser-Plasma Beat Wave Current Drive with an Eulerian Vlasov Code. *Nucl. Fusion*, Vol. 32, pp. 45-65

Groebner, R.J., Thomas, D.M. & Deranian, R.D. (2001). Evidence for Edge Gradients as Control Parameters of the Spontaneous High-Mode Transition. *Phys. Plasmas* , Vol. 8, pp. 2722-2732

Hirschman, S.P. (1978). The Ambipolarity Paradox in Toroidal Diffusion, Revisited. *Nucl. Fus.*, Vol.18, pp. 917- 927

Knorr, G., Joyce, G. & Marcus, J. (1980). Fourth-Order Poisson Solver for the Simulation of Bounded Plasmas. *J. Comput. Phys.*, Vol. 38, pp. 227-237

Manfredi, G., Shoucri, M., Dendy, R.O., Ghizzo, A. & Bertrand, P. (1996). Vlasov Gyrokinetic Simulations of Ion-Temperature-Gradient Driven Instabilities. *Phys. Plasmas* , Vol. 3, pp. 202-217

Pohn, E., Shoucri, M. & Kamelander G. (2005). Eulerian Vlasov Codes. *Comp. Phys. Comm*., Vol. 166, pp. 81-93

Pohn, E. & Shoucri, M. (2008). Collisionless Diffusion of Particles across a Magnetic field at a Plasma Edge in the Presence of Turbulence. *Proc. Vlasovia workshop*, in *Commun. Nonlinear Sci. Numer. Simul.*, Vol. 13, pp. 183-188

Shoucri, M., Lebas, J., Knorr, G., Bertrand, Ghizzo, A., Manfredi, G. & Christopher, I. (1997). Effect of Viscous Dissipation on the Generation of Shear Flow at a Plasma Edge in the Finite Gyroradius Guiding Center Approximation. *Physica Scripta,* Vol. 55, pp. 617-628

Shoucri, M., Pohn, E., Knorr, G., Bertrand, P., Kamelander, G., Manfredi, G. & Ghizzo, A. (2000). Charge Separation at a Plasma Edge in the Presence of a Density Gradient. *Phys. Plasmas,* Vol. 7, pp. 2517-2525

Shoucri, M. (2001). Numerical Simulation of Plasma Edge Turbulence due to *ExB* Flow Velocity Shear. *Czech. J. Phys*., Vol. 51, pp.1139-1151

Shoucri, M. (2002). Comments on 'Evidence for Edge Gradients as Control Parameters of the Spontaneous High- Mode Transition', *Phys. Plasmas,* Vol. 9, pp. 731-734

Shoucri, M., Gerhauser, H. & Finken, K.H. (2003). Numerical Simulation of the Formation of an Electric Field at a Plasma Edge in the Presence of a Density Gradient. *Proceedings of EPS 2003 30th Conference on Contr. Fusion and Plasma Phys.*, ECA Vol. 27A, P.1-170, St. Petersbourg, Russia, July 7-11

Shoucri, M., Gerhauser, H. & Finken, K.H. (2004). Study of the Generation of a Charge Separation and Electric Field at a Plasma Edge using Eulerian Vlasov Codes in Cylindrical Geometry. *Computer Physics Communications,* Vol. 164, pp. 138-149

Shoucri, M., Pohn, E.& Kamelander, G. (2005). Numerical Simulation of the Collisioless Diffusion of Particles across a Magnetic Field at a Plasma Edge. *Proceedings of EPS 2005 32nd Conference on Contr. Fusion and Plasma Phys.*, ECA Vol. 32D, P.-5.001, Tarragona, Spain, June 27-July 1

Shoucri, M. (2008a). *Numerical Solution of Hyperbolic Differential Equations*, Nova Science Publishers, ISBN 978-1-60456-459-4, New York

Shoucri, M. (2008b). Numerical Simulation For the Formation of a Charge Separation and an Electric Field at a Plasma Edge. *Proceedings of EPS 2008 35th Conference on Contr. Fusion and Plasma Phys.*, ECA Vol. 32D, P.-4.006, Hersonissos, Crete, Greece, June 9-13

Shoucri, M. (2008c). Eulerian Code for the Numerical Solution of the Vlasov Equation. *Proc. Vlasovia workshop*, in *Commun. Nonlinear Sci. Numer. Simul.*, Vol. 13, pp. 174-182

Shoucri, M. (2008d). Numerical Simulation of Wake-Field Acceleration using an Eulerian Vlasov Code. *Commun. Comp. Phys.*, Vol. 4, pp. 703-718

Shoucri, M. (2009a). The Application of the Method of Characteristics for the Numerical Solution of Hyperbolic Differential Equations, In: *Numerical Simulation Research Progress*, S.P. Colombo & C.L. Rizzo (Ed.), Nova Science Publishers, ISBN 978-1-60456-783-0, New York

Shoucri, M. (2009b). The Formation of a Charge Separation and an Electric Field at a Steep Plasma Edge. *Proceedings of EPS 2009 36th Conference on Contr. Fusion and Plasma Phys.*, ECA Vol.32D, P.- 4.105, Sofia, Bulgaria, June 29- July 3

Shoucri, M. (2011). In:*Eulerian Codes for the Numerical Solution of the Kinetic Equations of Plasmas.* M. Shoucri (Ed.), Nova Science Publishers, ISBN 978-1-61668-413-6, New York

Shoucri, R. & Shoucri, M. (2007). Applications of the Method of Characteristics for the Study of Shock Waves in Models of Blood Flow in the Aorta. *Cardiovasc. Eng.*, Vol. 7, pp.1-6

Sonnendrücker, E., Roche, J., Bertrand, P. & Ghizzo, A. (1999). The Semi-Lagrangian Method for the Numerical Resolution of the Vlasov Equation. *J. Comp. Phys.*, Vol. 149, pp. 201-220

Stix, T. (1973). Decay of Poloidal Rotation in a Tokamak Plasma. *Phys. Fluids*, Vol.16, pp.1260-1269

Strozzi, D., Shoucri, M., Bers, A., Williams, E.A. & Langdon, A.B. (2006). Vlasov Simulations of Trapping and Inhomogeneity in Raman Scattering. *J. Plasma Phys.*, Vol. 72, pp. 1299-1302

Waltz, R.E., Candy, J., Rosenbluth, M.N. & Hinton, F.L. (1999). Progress on a Full Radius Electromagnetic Gyrokinetic Code. *Proceedings of EPS 1999 26th Conference on Contr. Fusion and Plasma Phys.*, ECA Vol. 23J, pp. 1233-1236, Maastricht, Holland, June 14-18

Yanenko, N.N. (1971). *The Method of Fractional Steps*, Springer-Verlag, New York.

IntechOpen